JGR Atmospheres

RESEARCH ARTICLE
10.1029/2018JD028883

A Column Canopy-Air Turbulent Diffusion Method for Different Canopy Structures

Xuelong Chen[1,2], **William J. Massman**[3], **and Zhongbo Su**[2]

[1]Key Laboratory of Tibetan Environment Changes and Land Surface Processes, Institute of Tibetan Plateau Research, Chinese Academy of Sciences, Beijing, China, [2]Faculty of Geo-Information Science and Earth Observation, University of Twente, Enschede, Netherlands, [3]Rocky Mountain Research Station, U.S. Forest Service, Fort Collins, CO, USA

Key Points:
- Underestimation of sensible heat or overestimation of latent heat (evapotranspiration) by SEBS for a forest canopy is due to its overestimation of kB^{-1}
- Vertical variations of foliage density, foliage shielding, and foliage drag/heat transfer are used to build a column canopy-air exchange model
- The model accurately simulates heat flux for seven land covers by considering momentum and heat transfer efficiency in vertical layers

Correspondence to:
X. Chen,
x.chen@itpcas.ac.cn

Citation:
Chen, X., Massman, W. J., & Su, Z. (2019). A column canopy-air turbulent diffusion method for different canopy structures. *Journal of Geophysical Research: Atmospheres*, *124*, 488–506. https://doi.org/10.1029/2018JD028883

Received 24 APR 2018
Accepted 21 DEC 2018
Accepted article online 2 JAN 2019
Published online 17 JAN 2019

Abstract An accurate simulation of the sensible heat flux (H) over vegetation from thermal remote sensing requires an a priori estimate of roughness length and the excess resistance parameter kB^{-1}. Despite being the subject of considerable interest in hydrometeorology, there still does not exist a uniform method for estimating roughness length from remote sensing techniques. This study demonstrates a turbulent diffusion method to simulate canopy-air sensible heat. The performance of the roughness length scheme as described in Chen et al. (2013, https://doi.org/10.1175/JAMC-D-12-056.1) was examined by comparing simulated H to measured values at 28 flux tower stations, which include seven different land covers (needle forest, broadleaf forest, shrub, savanna, grassland, cropland, and sparsely vegetated land). The model predictions of H for grass, crop, and sparsely vegetated land compare favorably with observed values, when actual canopy height is given. H is significantly underestimated at forest sites due to a high value of kB^{-1}. Among the different physical representations for the canopy, canopy-soil mixture, and soil component, it is found that such a high kB^{-1} value is caused by the high kB^{-1} value for the canopy part. The reasons for this high kB^{-1} were investigated from canopy-air physical process of turbulent diffusion. This study introduces the vertical foliage density information into a column canopy-air turbulent diffusion model to include the different momentum and heat transfer efficiencies in the vertical canopy layers to enhance the thermal turbulent transfer intensity above the tall canopy. The new model has been verified to provide accurate simulation over different canopy structures.

1. Introduction

The sensible heat flux (H) between a forested surface and the atmosphere within the roughness sublayer can be estimated by means of the Monin-Obukhov similarity theory (MOST) when surface variables and synoptic meteorological information are available (Physick & Garratt, 1995):

$$H = k\,u_*\rho C_p(\theta_0-\theta_a)\left[\ln\left(\frac{Z_r-d_0}{z_{0h}}\right)-\Psi_h\left(\frac{Z_r-d_0}{L}\right)+\Psi_h\left(\frac{z_{0h}}{L}\right)+\int_{Z_r}^{Z_*}\frac{\Phi_s\,(1-\phi_s)}{Z}dz\right]^{-1}, \quad (1)$$

$$u_* = ku\left[\ln\left(\frac{Z_r-d_0}{z_{0m}}\right)-\Psi_m\left(\frac{Z_r-d_0}{L}\right)+\Psi_m\left(\frac{z_{0m}}{L}\right)+\int_{Z_r}^{Z_*}\frac{\Phi_u\,(1-\phi_u)}{Z}dz\right]^{-1}, \quad (2)$$

where k is the von Karman constant, u_* is the friction velocity, ρ is the density of air, C_p is the specific heat for air, θ_0 is the potential temperature at the surface, θ_a is the potential air temperature at height Z_r, d_0 is the zero plane displacement height, Ψ_h and Ψ_m are the stability correction functions for heat and momentum transfer, L is the Obukhov length, and z_{0h} and z_{0m} are the roughness length for heat and momentum transfer. Z_* is the height of the roughness sublayer. The integral terms on the right side of equations (1) and (2) are roughness sublayer corrections for sensible heat and momentum fluxes, which are necessary when Z_r is in the roughness sublayer above the canopy top.

Previous studies have shown that fluxes calculated from profiles by a method that integrated the roughness sublayer corrections were generally in good agreement with those measured by the eddy-covariance methods at forest sites (Mölder et al., 1999). Meanwhile, different forms of ϕ_s, ϕ_u, z_{0m}, and d_0 were used at different locations (Cellier & Brunet, 1992; De Ridder, 2010; Garratt, 1980; Mölder et al., 1999). No

uniform solution for these variables has been provided. This study aims to provide such a solution, which can be used for estimates of turbulent heat flux over any kind of canopy covers.

In addition, calculating H by means of similarity theory, z_{0h} and z_{0m} must be accurately determined. z_{0m} can be estimated by acquiring land surface physical roughness or geometric information for the canopy. z_{0h} can be derived from z_{0m} by adding an excess resistance for heat transfer kB^{-1} (where k is the same von Karman constant as in equation (2) and B is the Stanton number):

$$z_{0h} = \frac{z_{0m}}{\exp(k\,B^{-1})}, \tag{3}$$

z_{0m} and z_{0h} are defined as the heights (above the displacement height) where wind speed and temperature become equal to their surface values when the logarithmic profiles are extrapolated through the roughness sublayer. Consequently, z_{0h} and z_{0m} are a combination of the effects of the roughness sublayer and the actual vegetation-atmosphere interfacial transport, when the subroughness correction is added in the logarithmic profiles.

The difference in turbulent momentum and heat transfer efficiency is represented by kB^{-1}. Here we seek to exclude the effects of different turbulent transport in the roughness sublayer between momentum and heat on the calculation of the heat roughness length by adjusting kB^{-1}. kB^{-1} used in this study is calculated based on a Lagrangian model (Massman, 1999). The Lagrangian model takes into account the process of scalar diffusion at *near-field* and *far-field* (Mölder et al., 1999), as an alternative method for turbulent flux simulation within the canopy subroughness layer.

kB^{-1} has been the subject of increased interest in micrometeorology (Hong et al., 2012). Various empirical, semiempirical, and physical equations have been proposed to relate kB^{-1} with other more readily measurable variables, such as momentum roughness length, friction velocity, canopy height, and heat flux (Beljaars & Holtslag, 1991; Brutsaert & Sugita, 1996; Garratt & Hicks, 1973; Jensen & Hummelshøj, 1995; McNaughton & van den Hurk, 1995; Owen & Thomson, 1963; Qualls & Brutsaert, 1996; Thom, 1972; Verhoef, McNaughton, et al., 1997; Yang et al., 2003). After a comprehensive literature review, no commonly accepted kB^{-1} method has been found suitable to model the transitional regime from smooth to rough flow (Verhoef, De Bruin, et al., 1997) or from bare soil to low canopy and high canopy (Brutsaert, 2010), due to effects of different plant spacing and shapes.

The aim of this study is to derive a uniform kB^{-1} scheme, which is robust for heat flux calculation for high and low canopies. Recent observational studies reveal that kB^{-1} is dependent on environmental conditions, surface types, canopy structure (the sizes of the foliage elements and canopy height), and vegetation surface geometry (frontal area and surface density). For vegetated surfaces in particular, key variables are the mean canopy height (Chen et al., 2013; Saha, 2008), frontal surface area (Raupach, 1994), and the mean plant density. Improved characterization of the land surface canopies using satellite imagery is leading to improved estimates of kB^{-1}. Massman (1999) theoretically showed that kB^{-1} is controlled by leaf size, foliage distribution, leaf area index (LAI), and friction velocity. Based on plant phenology and Lagrangian theory (Massman, 1999), Su et al. (2001) built a kB^{-1} scheme from the work of Massman (1999), which can estimate individual contribution of bare soil, canopy, and mixed-canopy-soil to kB^{-1} seperately. The temporal variation of kB^{-1} and its dependency on plant functional types is considered by Su et al. (2001) as a function of LAI, canopy fraction, and canopy height, as all these canopy parameters can be provided by satellite remotely sensing. Meanwhile, our previous work (Chen et al., 2013) has updated $kB^{-1}$for the bare soil part, which has demonstrated a better kB^{-1}diurnal variation and more accurate simulation of H over four arid sites. The kB^{-1}parameterization method used in this study includes not only the schemes that set kB^{-1} as a function of the Reynolds number but also the schemes that express kB^{-1} as a function of plant phenology. Since the method relies on the characterization of the bulk canopy geometry, it offers an opportunity to estimate the local aerodynamic roughness that is also a function of the same physical properties. It can be independently used to predict kB^{-1}based on the vegetation characteristics, whereby the impact of the vegetation changes on kB^{-1}could be quantified and analyzed. The scheme has been applied to in situ observation (Chen et al., 2013; Ershadi et al., 2014), regional (Oku et al., 2007; Su et al., 2005), and continental scale (Chen et al., 2014; Vinukollu et al., 2011). The kB^{-1} model has a dependency on LAI, which can result in a seasonal variation in the kB^{-1} estimate. However, further efforts are still needed to improve its

applicability and accuracy over different land surface canopies (Chen et al., 2014). As $kB^{-1}$is only evaluated for sparse canopies or low canopies, direct application of this approach to dense or high canopies, such as a forest, induced unexplained errors in evapotranspiration, and surface fluxes estimations (Chen et al., 2013, 2014; Ershadi et al., 2014).

Relatively large roughness lengths for forest canopies can lead to an order of magnitude increase in its Reynolds number when compared to short canopies (Hong et al., 2012). A high Reynolds number results in a significant reduction in its modeled sensible heat fluxes over tall canopies due to the kB^{-1} parameterizations. This study attempts to assess the uncertainty in H for a tall forest canopy due to kB^{-1} parameterizations. The underestimation of H is due to an overestimation of kB^{-1}. In order to decrease kB_c (kB^{-1} of the canopy), the vertical foliage density profile was introduced to a column canopy-air turbulent transfer model to take into account momentum and heat transfer efficiency in different canopy vertical layers. Section 2 introduces the methodology and data collection for the model evaluation and verification. The equations used in the kB^{-1} column model are described in section 3. The inclusion of a vertical foliage drag coefficient, vertical foliage leaf area density, and foliage shelter factor are also introduced in this part. A new method for the calculation of the foliage heat transfer coefficient (closely related to canopy-air heat transfer) in the canopy resulted from this study, which improves the underestimation of turbulent heat flux. At the end, some applications and minor problems are discussed.

2. Methodology and Data Set

In what follows, we evaluate the performance of the turbulent flux parameterization scheme in our previous study by Chen et al. (2013). The subroughness length stability calibration is also used in the model for sensible heat simulation over forest sites. The methodology adopted here is different from the work on roughness sublayer stability correction ($\Psi_u(Z_r)$) by Harman and Finnigan (2008). The method from Physick and Garratt (1995) was used. The model evaluation is indirectly done by comparing H simulations with concurrent observations. The values of linear fitting slope, root-mean-square error (RMSE), and correlation coefficient (r) were used as a measure for the skill of the model.

We first tested the model simulation forced by flux-tower meteorological measurements from seven land cover units, evergreen needleleaf forest (ENF, five sites), deciduous broadleaf forest (DBF, six sites), shrub-land (SRB, three sites), savannas (SAV, four sites), grasslands (GRS, four sites), croplands (CRP, three sites), and barren or sparsely vegetated (BSN, three sites). Furthermore, measured H by the eddy covariance (EC) method at each station were used to assess the modeled H. Bias in the H simulation was diagnosed relating to the problem of kB^{-1}in presenting the canopy-air turbulent transfer process, as it is assumed that the input data from flux towers are accurate without bias. After diagnosing the problems in the model, the model structure was adjusted from a one-foliage layer to a multifoliage layer, which provides the possibility of including the impact of vertical variations in foliage leaf area density, foliage shelter factor, and foliage heat transfer coefficient.

To calculate H, the air temperature, pressure, relative humidity, wind speed, and land surface temperature (LST) from the stations were needed. Here LST was computed from measured upward longwave radiation and downward longwave radiation using the Stefan-Boltzmann equation. The Moderate Resolution Imaging Spectroradiometer (MODIS) emissivity (MOD11C3 V5 and MYD11C3 V5) was used to calculate in situ LST (Chen et al., 2017). In order to produce accurate estimates of H, we used as much as possible available observational information. Years of meteorological data and ancillary parameters were collected from 28 flux stations to perform the H simulations. The canopy height at ENF sites varies from 11 to 35 m with different tree density and space. DBF sites have canopy heights between 24 and 30 m. SAV stations have canopy height of 4–15 m. SRB stations have canopies from 0.5- to 3-m height. The bare soil stations were also included as a reference for nonvegetated area, which has a relatively homogenous and smooth surface without interruption from canopy roughness elements.

2.1. Data Collection and Processing

Flux tower data used in this paper were collected from the AmeriFlux Level 2 database (ftp://cdiac.ornl.gov/pub/ameriflux/data/Level2, April 2010), Ozflux Level 2 (http://www.ozflux.org.au/index.html), and China flux sites. Meteorological variables are measured at all flux towers. Other variables, such as net radiation

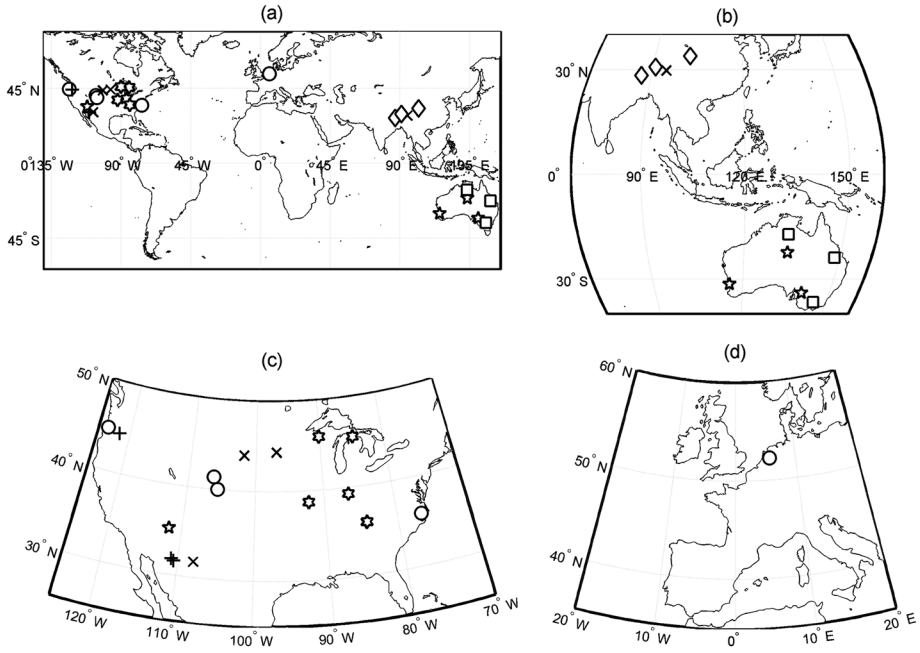

Figure 1. Geolocation of evergreen needleleaf forest (labeled by circle), deciduous broadleaf forest (hexagon), shrub-land (square), savannas (pentagram), grasslands (cross), croplands (plus), and barren or sparsely vegetated (diamond) flux tower stations on different continents.

and ground heat flux, are measured at a limited number of towers. The final selection of sites represents a number of typical biomass and climates. Seventeen flux sites were selected from AmeriFlux, six sites from Ozflux, four sites from the Tibetan Plateau in the Third Pole Environment database (Ma et al., 2008), and one site in the Netherlands, as these stations have provided all necessary measurements (including surface radiation components, air temperature, pressure, humidity, wind speed, and turbulent fluxes) to run and verify the model. The locations of the 28 sites are shown in Figure 1. The detailed coordinates and elevations of these sites are listed in Table 1.

The researchers at the flux sites have done a data quality assessment and controlling process to their flux data, such as spike detection, tilt-correction, and WPL-corrections (Webb et al., 1980). Data quality control is also done by Ameriflux, Ozflux, and Chinaflux network contributors. The data set has a temporal resolution of 30 min. As gap filling implies an additional error added in the data, which might influence the results of analysis, only the available measured data were used without gap filling. Physically unreasonable values were removed. The model is evaluated with H measurement only under dry conditions as EC gas analyzers are not reliable during rain events due to disturbance of the infrared signal by droplets on the sensor (Burba et al., 2010). Therefore, data from any days with precipitation are removed from the analysis. H with friction velocities less than a critical value of 0.01 m/s were also excluded from the analysis.

2.2. Canopy Information at the Flux Sites

The importance of canopy structure (stem, crown height and width, the number of plants per unit ground area, and distance between the plants) to roughness length has been discussed by Schaudt and Dickinson (2000). We also believe that more canopy structure information would improve the modeling of turbulent momentum and heat transfer between the canopy surface and atmosphere. The model used here needs some independent canopy variables (e.g., canopy height, canopy fraction, LAI, and normalized difference vegetation index [NDVI]), which were retrieved from satellite data. These canopy variables are necessary for kB^{-1} calculation at regional scale or in situ station scale. Forest canopy height is typically considered constant, while for other canopies, for example, crop, grass, and shrub, their heights can change largely within a season. The height information for tall canopy (e.g., forest and savanna) is obtained from the description on the

Table 1
Eddy Covariance Site Information

Site no.	Name	Lat (deg)/Lon (deg)	Land cover	*h* (m)	Period	Site elevation (m)	Meteorological measurement height (above ground floor)
1	Speulderbos	52.25225, 5.6905	ENF	32	January 2009 to December 2009	52	Upward longwave radiation 35 m, wind speed 46 m, eddy covariance 46 m, air temperature 45 m
2	US-NC2	35.8031, −76.6685	ENF	18.2	January 2008 to December 2008	5	Upward longwave radiation 22.5 m, wind speed 22.5 m, eddy covariance 22.5 m, air temperature 22.5 m
3	US-GLE	41.3644, −106.2390	ENF	13	October 2010 to December 2010	3190	Upward longwave radiation 24.3 m, wind speed 25.7/22.5 m, eddy covariance 22.5 m, air temperature 23.7 m
4	US-MRf	44.6465, −123.5500	ENF	34	January 2009 to December 2009	236	Upward longwave radiation 37 m; wind speed 38.3,39.5 m; eddy covariance 38.3 m; air temperature 4, 38 m
5	US-NR1	40.0329, −105.5400	ENF	11.5	January 2011 to December 2011	3023	Upward longwave radiation 25.5 m, wind speed 21.5 m, eddy covariance 21.5 m, air temperature 21.5 m
6	US-UMB	45.5598, −84.7138	DBF	22	January 2008 to May 2008	234	Upward longwave radiation 46 m, wind speed 46 m, eddy covariance 48 m, air temperature 46 m
7	US-ChR	35.9311, −84.3324	DBF	30	January 2010 to December 2010	286	Upward longwave radiation 43 m, wind speed 43 m, eddy covariance 43 m, air temperature 43 m
8	US-MOz	38.7441, −92.2000	DBF	18.5	June 2009 to December 2009	219	Upward longwave radiation 31 m, wind speed 31.4 m, eddy covariance 31 m, air temperature 31.4 m
9	US-MMS	39.3232, −86.4130	DBF	27	January 2010 to December 2010	275	Upward longwave radiation 46 m, wind speed 46 m, eddy covariance 48 m, air temperature 46 m
10	US-WBW	35.9588, −84.2874	DBF	25	January 2004 to December 2004	343	Upward longwave radiation 38 m, wind speed 36.6 m, eddy covariance 36.9 m, air temperature 38.2 m
11	US-WCr	45.9059, −90.0799	DBF	24.2	January 2005 to December 2005	515	Upward longwave radiation 29.6 m, wind speed 29.6 m, eddy covariance 29.6 m, air temperature 29.6 m
12	US-Aud	31.5907, −110.5092	SRB	hcMin = 0.002; hcMax = 0.5	January 2005 to December 2005	1469	Upward longwave radiation 1.6 m, wind speed 2 m, eddy covariance 3 m, air temperature 2 m
13	Us-Me6	44.3232, −121.600	SRB	7.5 m	January 2010 to December 2010	966	Upward longwave radiation 10 m, wind speed 12 m, eddy covariance 12 m, air temperature 10 m
14	US-SRM	31.8214, 110.8661	SRB	2.5	January 2010 to December 2010	1116	Upward longwave radiation 12 m, wind speed 12 m, eddy covariance 12 m, air temperature 12 m
15	Gingin	−31.375, 115.650	SAV	6.8	January 2012 to December 2012	1469	Upward longwave radiation 15 m, wind speed 15 m, eddy covariance 15 m, air temperature 15 m
16	Calperum	−34.002, 140.589	SAV	5.5	January 2011 to December 2011	4520	Upward longwave radiation 20 m, wind speed 20 m, eddy covariance 20 m, air temperature 20 m
17	Ti Tree East	−22.287, 133.640	SAV	4.5	July 2012 to December 2013	553	Upward longwave radiation 9.9 m, wind speed 8.28 m, eddy covariance 9.81 m, air temperature 9.81 m
18	US-Fmf	35.1426, −111.7270	SAV	15	July 2010 to December 2010	2160	Upward longwave radiation 23 m, wind speed 23 m, eddy covariance 23 m, air temperature 23 m
19	Linzhi	29.7622, 94.7417	GRS	hcMin = 0.0012; hcMax = 0.8	February 2007 to Octobr 2007	3327	Upward longwave radiation 1.5 m, wind speed 5 m, eddy covariance 3.2 m, air temperature 4.9 m

Table 1 *(continued)*

Site no.	Name	Lat (deg)/Lon (deg)	Land cover	h (m)	Period	Site elevation (m)	Meteorological measurement height (above ground floor)
20	US-Br1 (Brookings)	44.3453, −96.8362	GRS	hcMin = 0.0012; hcMax = 0.4	January 2009 to December 2009	994	Upward longwave radiation 2 m, wind speed 4 m, eddy covariance 3 m, air temperature 4 m
21	US-Ctn	43.9500, −101.846	GRS	hcMin = 0.0012; hcMax = 0.3	January 2007 to December 2007	744	Upward longwave radiation 2 m, wind speed 4 m, eddy covariance 3 m, air temperature 4 m
22	US-Wkg	31.7365, −109.941	GRS	hcMin = 0.0012; hcMax = 0.5	January 2010 to December 2010	1531	Upward longwave radiation 1.5 m, wind speed 2.1 m, eddy covariance 2.1 m, air temperature 1.5 m
23	Riggs Creek	−36.6560, 145.5760	CRP	hcMin = 0.002; hcMax = 1	January 2011 to December 2011	152	Upward longwave radiation 10 m, wind speed 2.5 m, eddy covariance 2.5 m, air temperature 2.5 m
24	Daly Pasture	−17.150, 133.350	CRP	hcMin = 0.5; hcMax = 1.5	January 2011 to December 2011	102	Upward longwave radiation 15 m, wind speed 15 m, eddy covariance 15 m, air temperature 15 m
25	Arcturus	−23.8587, 148.4746	CRP	hcMin = 0.01; hcMax = 0.8	January 2011 to December 2011	4700	Upward longwave radiation 5.6 m, wind speed 5.6 m, eddy covariance 6.7 m, air temperature 5.6 m
26	QOMS	28.358209, 86.949638	BSN	hcMin = 0.0012; hcMax = 0.1	March 2007 to December 2007	4276	Upward longwave radiation 1.5 m, wind speed 5 m, eddy covariance 3 m, air temperature 5 m
27	Nam Co	30.7699, 90.9636	BSN	hcMin = 0.0012; hcMax = 0.01	March 2007 to December 2007	4730	Upward longwave radiation 1.5 m, wind speed 5 m, eddy covariance 3 m, air temperature 5 m
28	Maqu	33.8872, 102.1406	BSN	hcMin = 0.0012; hcMax = 0.5	April 2009-May 2010	3439	Upward longwave radiation 1.5 m, wind speed 10 m, eddy covariance 3 m, air temperature 10 m

Fluxnet website or by contact with the site PIs. The height for low canopy (h) is computed from MODIS NDVI data (MOD13C2) using the following equation (Chen et al., 2013):

$$h = h_{\min} + \frac{h_{\max} - h_{\min}}{(\mathrm{NDVI}_{\max} - \mathrm{NDVI}_{\min})} * (\mathrm{NDVI} - \mathrm{NDVI}_{\min}), \tag{4}$$

where $h_{\max}$ and $h_{\min}$ are the measured maximum and minimum canopy height, $h_{\min}$ is set to 0.0012, and $h_{\max}$ is the highest canopy height for a specific canopy in 1 year. More information about $h_{\max}$ for the estimate of regional canopy height could be found in Chen et al. (2014). The NDVI canopy height method is designed for global remote sensing flux calculation, although NDVI has no direct relation with canopy height. NDVI data quality has a significant influence on canopy height and even more on the accuracy of turbulent heat flux. In order to eliminate the noise in daily NDVI time series, monthly NDVI data sets were used.

3. Model Introduction and Improvements

3.1. Model Introduction

The integration for ϕ_s and ϕ_u goes from a certain height in the roughness sublayer up to the top of the roughness sublayer. There are many methods that could be used to calculate ϕ_s and ϕ_u (Cellier & Brunet, 1992; De Ridder, 2010; Flerchinger et al., 2012; Harman & Finnigan, 2007). Stability functions in the roughness sublayer are still a thorny issue in the literature. There could be large uncertainties associated with these methods. The method developed by Physick and Garratt (1995) (PG95) is used. In unstable conditions ($\zeta = z/L \leq 0$)

$$\Phi_s = P_r(1-9\zeta)^{-0.5}, \tag{5}$$

$$\Phi_u = (1-15\zeta)^{-0.25}, \tag{6}$$

$$\phi_s = \phi_u = 0.5\ \exp(0.7\ Z/Z_*), \tag{7}$$

and stable conditions ($\zeta > 0$)

$$\Phi_s = P_r + 4.7\zeta, \tag{8}$$

$$\Phi_u = 1 + 4.7\zeta, \tag{9}$$

$$\phi_u = \phi_s = 0.5\ \exp(0.7\ Z/Z_*), \tag{10}$$

with P_r is the Prandtl number. An approximate roughness-sublayer height can reach three to eight times the stand height (Garratt, 1978). Cellier and Brunet (1992) take Z_* as the height of two times the canopy height. This study uses $Z_* = 3.45\ h$.

The kB^{-1} scheme developed by Su et al. (2001) is constructed using the *localized near-field (LNF)* Lagrangian theory (Raupach, 1989), due to it is consistent with the observed within-canopy counter gradient canopy flow. The LNF model for kB^{-1} is a combination of a far-field and a near-field temperature profile, with a canopy source function and leaf boundary layer resistance, the canopy momentum transfer model, a canopy turbulence model, and soil boundary layer resistance (Massman, 1999). This makes the kB^{-1} used in this study a combination of a three source method. It takes into account the vegetation, soil component and the combined effects of the canopy and soil in a single source approach by using the fraction of soil and canopy coverage as their weighting coefficients (Su, 2002). The model describes the canopy, soil, and combined canopy-soil boundary layer effects on kB^{-1}. The first term kB_c^{-1} follows the full canopy-only model of Choudhury and Monteith (1988), which is used to parameterize the canopy-air exchange resistance. The second term is that of Brutsaert (1982) for a bare soil surface, used for describing soil-air turbulent exchange resistance. The third term is used to describe the interaction between the canopy and soil or could be taken as a description of canopy soil interaction resistance. The kB^{-1} from Su (2002) is

$$kB^{-1} = {f_c}^2\ kB_c^{-1} + {f_s}^2\ kB_s^{-1} + 2{*}f_c f_s\ kB_m^{-1}, \tag{11}$$

where f_c is the fractional canopy coverage and f_s is that of soil (f_s=1-f_c). kB_c^{-1} is kB^{-1} of the canopy only, which is expressed as

$$kB_c^{-1} = \frac{k\ C_d}{4\ C_t\ \frac{u_*}{u(h)}\ (1-e^{-n_{ec}/2})}, \tag{12a}$$

C_d is the foliage drag coefficient, C_t is the heat transfer coefficient of the leaf, and n_{ec} is the wind speed profile extinction coefficient in the canopy. $\frac{u_*}{u(h)}$ is calculated by a submodel of momentum transfer in canopy:

$$\frac{u_*}{u(h)} = C_1 - C_2 \exp(-C_3\ \zeta(h)), \tag{12b}$$

$$n_{ec} = \frac{\zeta(h)}{2\times(C_1 - C_2\ \exp(-C_3\ \zeta(h)))^2}, \tag{12c}$$

where $C_1 = 0.320$, $C_2 = 0.264$, and $C_3 = 15.1$. The Surface Energy Balance System (SEBS) model version (Su, 2002) (Su02) uses $\zeta(h) = C_d$ LAI, which is different with that of Su et al. (2001) using a with-in canopy wind profile information. A column canopy-air turbulent transfer model is introduced by this study to calculate $\zeta(h)$ (see section 3.3).

kB_m^{-1} describes the combined canopy and soil boundary layer effects on kB^{-1} (soil-plant interaction component) and is a function of Reynolds number.

$$kB_m^{-1} = \frac{k\frac{u_* z_{0m}}{u(h)\ h}}{C_t^*}, \tag{13a}$$

The heat transfer coefficient of the soil (C_t^*) is given by

$$C_t^* = \mathrm{Pr}^{-2/3}\,\mathrm{Re_s}^{-1/2}, \tag{13b}$$

where $P_r = 0.71$, suggested by Massman (1999) and the roughness Reynolds number for soil $\mathrm{Re_s} = h_s\, u_*/\vartheta$, with h_s being the roughness height of the soil (0.004 m). The kinematic viscosity of the air $\vartheta = 1.327 \times 10^{-5}(p_0/p)(T/T_0)^{1.81}$ (Massman, 1999), with p and T being the ambient pressure and temperature, p_0=101.3 kPa, and T_0=273.15 K.

kB_s^{-1} is the bare soil part, which is calculated according to Brutsaert (1982) from Su et al. (2001) as

$$kB_s^{-1} = 2.46\ \mathrm{Re_s}^{1/4} - \ln(7.4), \tag{14a}$$

In our previous work of Chen et al. (2013)(Chen13), kB_s^{-1} is revised as following, while keeping kB_m^{-1} and kB_c^{-1} the same as the original version in Su et al. (2001) and SEBS model:

$$kB_s^{-1} = \ln\left(\frac{z_{0m\_s}}{z_{0h\_s}}\right), \tag{14b}$$

$$z_{0h\_s} = \frac{70\,\vartheta}{u_{s*}} \exp\left(-\beta\, {u_{s*}}^{0.5} {\theta_{s*}}^{0.25}\right), \tag{14c}$$

where β equals 7.2 $\mathrm{s}^{0.5} \cdot \mathrm{m}^{-0.5} \cdot \mathrm{K}^{-0.25}$ and u_{s*} and θ_{s*} are the soil surface friction velocity and friction temperature. z_{0m_s} is momentum roughness length for soil. The detailed calculation method for z_{0h_s}, θ_* and u_* can be found in Yang et al. (2002). Here z_{0m_s} is set to equal to h_s (0.004 m). The air temperature, wind speed, humidity, and pressure used to calculate kB_s^{-1} are assumed to the same as that of a soil-canopy mixed pixel. So that the canopy and soil part experience the same temperature and humidity as well as other meteorological forcing. kB_s^{-1} is computed with u_*(via $\mathrm{Re_s} = h_s\, u_*/\vartheta$) in Su02, shown by equation (14a), while Yang et al. (2002) takes into account the diurnal variation in u_{s*} and θ_{s*}. θ_{s*} is derived with the land-air temperature gradient, which means that the strong diurnal variation in the temperature gradient is included in equation (14b), and explains why it could provide a better H estimate than equation (14a).

3.2. Problems of the kB^{-1} Scheme Over Forest Canopies

In the following we will analyze the model structure, which can be related to the errors in H simulation. Figure 2 shows a comparison of sensible heat flux between Su02, Chen13 simulation, and flux tower observation for two forest sites. The result from Su02 is similar to Chen13 at forest sites. However, Chen13 has a better performance than Su02 at other canopy covers. Speulderbos and US-UMB are taken as a demonstration site for ENF and DBF, respectively. H simulated by the model is much lower than observations at both sites. The phenomena shown by the two sites are similar to all other needleleaf and broadleaf forest sites. Meanwhile, the model has an accurate estimate at GRS, CRP, and BSN. The roughness sublayer correction is also included in the simulation, which is annotated by *Su02 + PG95* and *Chen13 + PG95* in Figure 2.

In order to diagnose the underestimation of H at forest sites by the model, Figure 3 shows the temporal variation of half-hourly values of kB^{-1} in 2009 at the Speulderbos ENF site (Su et al., 2009). Two similar versions of kB^{-1} from Su02 and Chen13 were included. Seasonal variations in the three parts of kB^{-1} were shown separately. The instantaneous values of kB_c^{-1}, kB_m^{-1}, kB_s^{-1}, and kB^{-1} proved to be highly variable. kB_c^{-1} and kB_m^{-1} have a distinct seasonal pattern, with low values in summer due to a high leaf density and high ones in winter. Both kB_s^{-1} calculated by Su02 and Chen13 show that the highest values are usually around midday and the lowest ones in the morning, which are consistent with reports from other studies for bare ground surfaces (Feng et al., 2012; Sun, 1999; Verhoef, De Bruin, et al., 1997; Wang & Ma, 2011). Both models can give negative kB_s^{-1} values during nighttime, a phenomena which is often observed for relatively smooth surfaces (Wang & Ma, 2011; Yang et al., 2003). However, the daytime average kB_s^{-1} from Su02 is about 7.5, much higher than the 1 of Chen13, causing a higher kB^{-1} than Chen13. The average kB^{-1} from Su02 is about

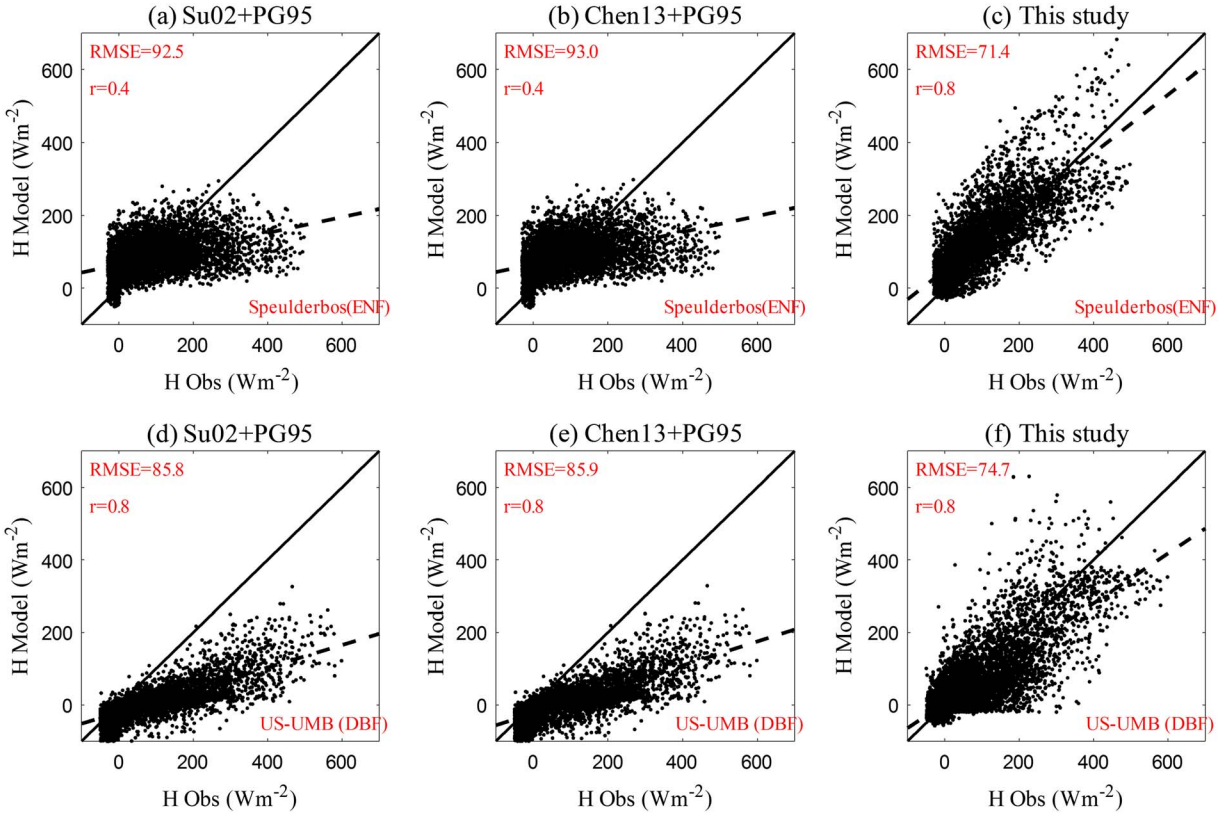

Figure 2. Comparison between sensible heat simulated by Su02 + PG95, Chen13 + PG95, and this study against observations at Speulderbos evergreen needleleaf forest (ENF) and US-UMB deciduous broadleaf forest (DBF).

5.4, while Chen13 estimated it to be 5.1. Bosveld (1999) reported kB^{-1} around 0 for ENF at Speulderbos. Mölder et al. (1999) also found approximately the same low value for a boreal pine-spruce forest. A higher kB^{-1} will result in a higher heat transfer resistance, which causes lower sensible heat flux and vice versa. It can be deduced that the underestimation of sensible heat at ENF is due to an overestimation of kB^{-1}. Chen13 gives a decreased kB_s^{-1} value, but the weight coefficients (f_s^2) for kB_s^{-1} are too low, which causes Chen13 to fail to provide a *true* estimation of kB^{-1} over forest sites. Relatively high canopy fraction at forest sites results in a high contribution of kB_c^{-1} to kB^{-1}. kB_c^{-1} values change between 7 and 9, which are much higher than 2, as usually assumed to hold for vegetation (Garratt & Hicks, 1973). Therefore, high kB_c^{-1} values result in high kB^{-1} and high canopy resistance, which result in low H at ENF sites.

The daytime average kB_s^{-1} at a DBF site produced by Su02 is about 6.0 (Figure 4), much higher than that of Chen13. Due to its high kB_s^{-1} values, Su02 also gives a high kB^{-1} than Chen13. Su02 produced an average kB^{-1} value of 5.5 in January and December and value of 5 during June to September. Lower kB^{-1} from Chen13 means that the heat transfer resistance from the soil will also be lower than Su02. This explains why Chen13 has solved the underestimates of sensible heat for BSN, CRP, and GRS sites (Chen et al., 2013). Despite that Chen13 gives a relatively higher H than that of Su02, H simulation is still lower than the true values. The contribution from kB_c^{-1} to the variation of kB^{-1} is more important than the other two kB^{-1} components at DBF sites, as the canopy resistance is significant for areas of full canopy cover.

As the scale of the turbulence is approximately that of the height of the canopy, turbulence over forest sites is more intensive than that over short canopies and causes turbulent heat exchange to be more efficient for forest sites. The *canopy convector effect* (Rotenberg & Yakir, 2010) can effectively reduce the aerodynamic resistance, and forests would have intrinsically lower aerodynamic resistance to heat transfer than short canopies (Banerjee et al., 2017). Results from both ENF and DBF sites show the necessity for revising the scheme for kB_c^{-1} in order to decrease the canopy heat transfer resistance for forest sites. The low turbulent heat transfer

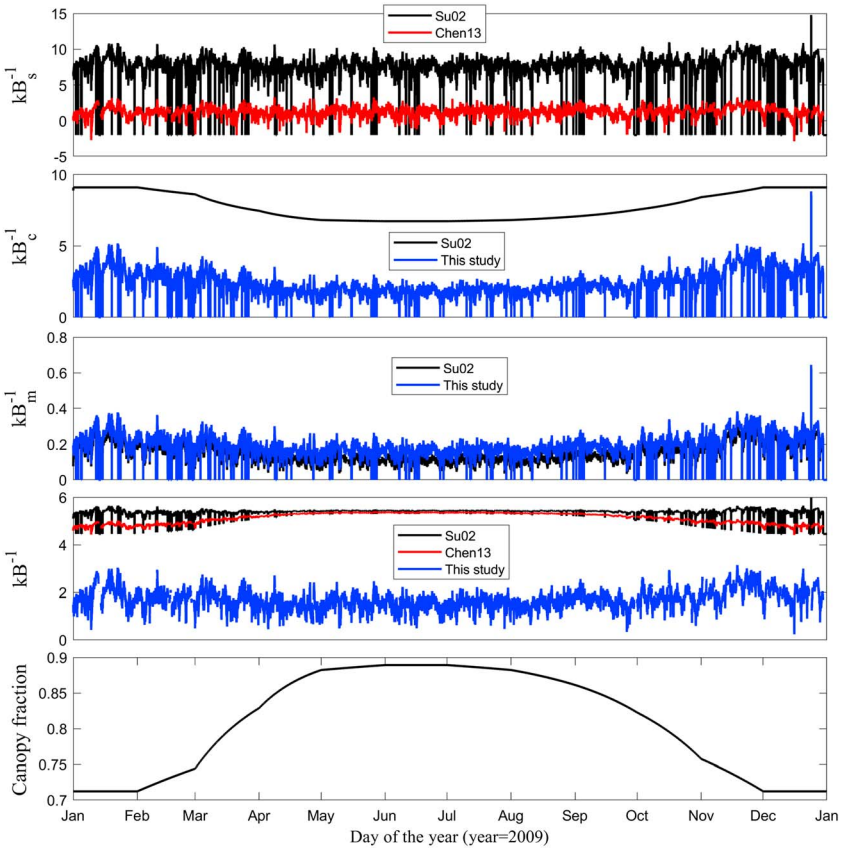

Figure 3. Time series of kB_c^{-1}, kB_s^{-1}, kB_m^{-1}, kB^{-1}, and f_c at Speuderbos evergreen needleleaf forest station derived by Su02 (dark line), Chen13 (red line), and this paper (blue line). The time resolution for the four kB^{-1} variables is half-hour.

resistance over forest could in turn enhance sensible heat as the forest and surface air temperature gradient is quite low (Rotenberg & Yakir, 2010). This explains why a canopy-soil-air heat transfer resistance scheme that is valid for short canopy cannot work well at forest sites.

A similar study of kB_c^{-1} values at SRB, SAV, GRS, and CRP (not shown here) sites has also been conducted. The common conclusion is that the underestimation of H is due to higher kB_c^{-1}. While Chen13 produced a lower kB_s^{-1} than Su02 for all the land surfaces, which makes the model produce better estimates of H at ENF, DBF, GRS, CRP, and BSN sites, the underestimation for forest sites is not fully solved even by adding the roughness sublayer correction from Physick and Garratt (1995). Thus, a more robust model needs to be provided for forest canopies.

When land surface changes from bare soil, to grass, shrub, and forest canopy, the frictional resistance to surface airflow will increase, because the roughness of the underlying surface increases. While the boundary layer between near-surface and the atmosphere becomes more complex, the turbulence within the roughness sublayer above the canopy is affected more by vegetation height, vegetation horizontal structure, and other canopy related factors. As a result, the kB_c^{-1} estimated only by using LAI in Su02 and Chen13 may not be sufficient for different vegetated land surfaces. Thus, some other critical vegetation characteristics and wind factors should be taken into account for kB^{-1} calculation, which will be the subject of next section. Considering Chen13 has a better or equal performance than Su02 for 5 out of 7 land covers (ENF, DBF, GRS, CRP, and BSN), the following work will be based on Chen13 kB^{-1} version to make a further enhancement.

The model version in Chen13 is a simple version of Su et al. (2001) and is similar to the one used in Su02 (or SEBS model). Neither Chen13 nor Su02 include a submodel of within canopy wind profile. Su02 uses an effective foliage heat and momentum drag coefficient ($C_d = 0.2$, $C_t = 0.01$), neglecting the variation of turbulent transfer efficiency within the canopy. Both Su02 and Chen13 adopt an idea of *big leaf*, without

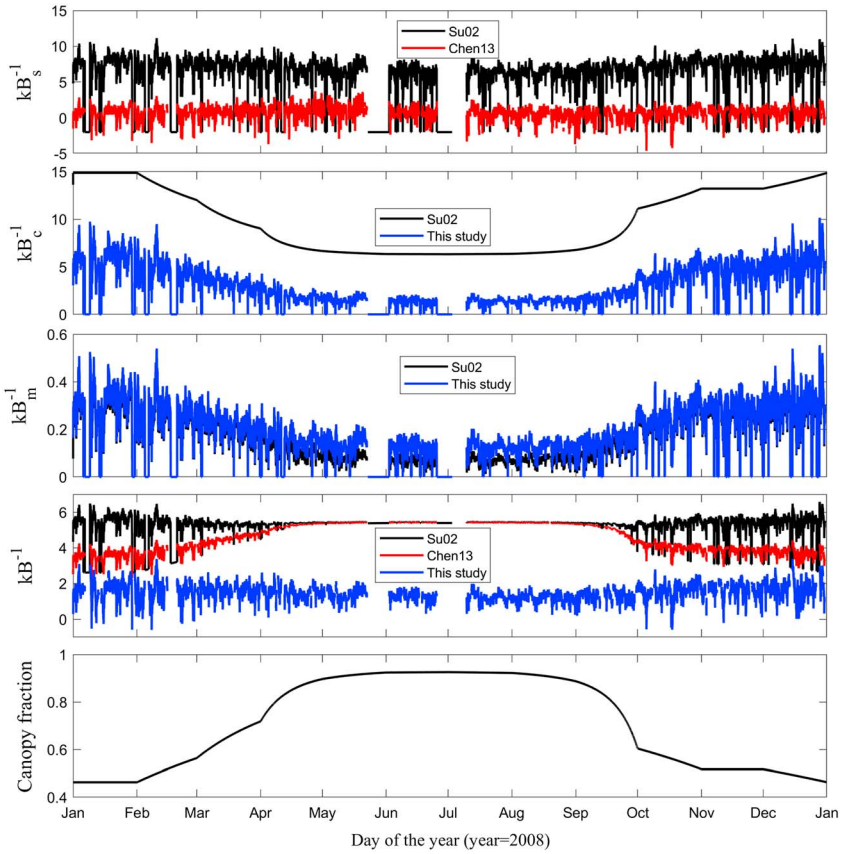

Figure 4. Time series of kB_c^{-1}, kB_s^{-1}, kB_m^{-1}, kB^{-1}, and f_c for US-UMB deciduous broadleaf forest station derived by Su02 (dark line) Chen13 (red line), and this paper (blue line). The time resolution for the four kB^{-1} variables is half-hour.

wind information within the canopy, which will influence the heat and mass transfer between canopy and air above it. From the foregoing study it is clear that describing the vertical wind profile within the canopy is necessary for simulating turbulent heat transfer over the forest canopy. Therefore, a submodel of within canopy wind has been included to make this model a column canopy-air turbulent transfer model as follows.

3.3. Model Reconstruction and Improvements

Table 2 shows a list of variables used in SEBS and the model developed by this study. The main difference is about the introduction of vertical foliage density, foliage drag coefficient in the canopy, foliage heat transfer efficiency in the canopy, foliage shelter factor for momentum, and subroughness correction in the model developed by this study. The method for calculation of displacement height is also changed. Below is the detailed explanation on these revisions.

3.3.1. A Column Canopy-Air Turbulent Transfer Model

Within the canopy the wind speed is modeled as an exponential function of cumulative leaf drag area per unit planiform area after Albini (1981):

$$\frac{u(z)}{u(h)} = e^{-n_{ec}\,(1-\zeta(z)/\zeta(h))}, \tag{15}$$

where z is the height above the soil surface and in the canopy and $\zeta(z)$ is the cumulative leaf drag area per unit planform area:

$$\zeta(z) = \int_0^z \left[a\left(z'\right)\, C_d^v\left(z'\right)\, P_m^v\left(z'\right)\right] dz', \tag{16}$$

$\zeta(z)$ changes with the height in the canopy (z). Here $a(z')$ is the vertical foliage leaf area density function, $C_d^v\left(z'\right)$ is the foliage drag coefficient as a function of height within the canopy, and $P_m^v\left(z'\right)$ is the foliage shelter factor for momentum. To have a sounder description of turbulent process in the canopy, the following

Table 2
Parameters or Intermedium Variables Used in SEBS and the Model Developed in This Study

Symbol	Description	SEBS	This study
k	von Karman constant	0.4	0.4
C_d	foliage drag coefficient	0.2	0.2
z_{0m_s}	soil roughness length	0.009 m	0.004 m
Pr	Prandtl number	0.71	0.71
h_s	soil roughness height	0.009	0.004 m from Chen et al. (2013)
l	the characteristic leaf length scale	Not used	0.01 m
f_c	fractional canopy coverage	$(\text{NDVI-NDVI}_{\min})^2/(\text{NDVI}_{\max}-\text{NDVI}_{\min})^2$	$1-\exp(-0.5\ \text{LAI})$
f_s	fraction of bare soil	$1-f_c$	$\exp(-0.5\ \text{LAI})$
h	canopy height	No specific solution.	$h_{\min\text{LCT}}+\frac{h_{\max\text{LCT}}-h_{\min\text{LCT}}}{(\text{NDVI}_{\max}-\text{NDVI}_{\min})}(\text{NDVI}-\text{NDVI}_{\min})$
ξ	Nondimensional height above soil surface	Not used	Varies from 0 (soil surface) to 1 (canopy top)
C_t	heat transfer coefficient for the leaf	0.01	$\overline{C_t^v(z)}$
$C_t^v(\xi)$	foliage heat transfer efficiency in the canopy	Not used	$[\,u*/u(h)]^{0.5}*Pr^{-0.67}*\text{Re}*(\xi)^{-0.5}$
C_t^*	heat transfer coefficient of the soil	$\text{P}_r^{-2/3}\text{Re}_\text{s}^{-1/2}$	$\text{P}_r^{-2/3}\text{Re}_\text{s}^{-1/2}$, with different Re_s value
Re_s	Reynolds number for soil	$h_s\,u*/\vartheta$	$h_s\,u*/\vartheta$, with different h_s value
$\text{Re}*(\xi)$	local canopy Reynolds number	Not used	$l\,u(\xi)/\vartheta$
$u(\xi)$	wind speed in the canopy	Not used	$u(h)\ \exp^{-n_{ec}\ (1-\zeta(\xi)/\zeta(h))}$
$u(h)$	wind speed at the canopy top	Not used	$U\left(\frac{\log((h-d0)/z_{0m})}{\log((h+10-d0)/z_{0m})}\right)$
ϑ	kinematic viscosity of the air	$1.327\times10^{-5}\left(\frac{p_0}{p}\right)\left(\frac{T}{T_0}\right)^{1.81}$, p_0=101.3 kPa, and T_0=273.15 K	Same as SEBS
$u*$	friction velocity	$ku\left[\ln\left(\frac{Z_r-d_0}{z_{0m}}\right)-\Psi_m\left(\frac{Z_r-d_0}{L}\right)+\Psi_m\left(\frac{z_{0m}}{L}\right)\right]^{-1}$	$ku\left[\ln\left(\frac{Z_r-d_0}{z_{0m}}\right)-\Psi_m\left(\frac{Z_r-d_0}{L}\right)+\Psi_m\left(\frac{z_{0m}}{L}\right)+\Psi_u(Z_r)\right]^{-1}$
C_p	specific heat for moist air	1846 Q + (1-Q) 1005	1846 Q + (1-Q) 1005
θ_0	potential temperature at the land surface	$\text{LST}(p_0/p)^{0.286}$,	$\text{LST}(p_0/p)^{0.286}$,
d_0	Zero plane displacement height (m)	$h(1-1/(2\,n_{ec})(1-\exp(-2\,n_{ec})))$	$h\left(1-\frac{u_*^2(0)}{u_*^2(1)}\right)\frac{\int_0^1[u_*^2(\xi)/u_*^2(1)]\xi d\xi}{\int_0^1[u_*^2(\xi)/u_*^2(1)]d\xi}$
z_{0h}	heat roughness length	$z_{0h}=\frac{z_{0m}}{\exp(kB^{-1})}$	Same as SEBS, but with different z_{0m} and kB^{-1}.
z_{0m}	momentum roughness length	$\left(1-\frac{d_0}{h}\right)e^{-k\ u(h)/u*}$	Same as SEBS, but with different $\frac{d_0}{h}$ and $\frac{u*}{u(h)}$ method
kB^{-1}	excess resistance	$f_c^{\,2}\,kB_c^{-1}+f_s^{\,2}\,kB_s^{-1}+2f_cf_s\,kB_m^{-1}$	Same as SEBS, but with different kB_c^{-1}, $kB_m^{-1}$and kB_s^{-1}
kB_c^{-1}	kB^{-1} of the canopy	$\frac{kC_d}{4C_t\frac{u*}{u(h)}(1-e^{-nec/2})}$	Same as SEBS, with different values for C_t, $\frac{u*}{u(h)}$, and n_{ec}
kB_s^{-1}	kB^{-1} of bare-soil	$2.46\ \text{Re}_\text{s}^{1/4}-\ln(7.4)$	$\log\left(\frac{z_{0ms}}{\frac{70\ \vartheta}{u*}\exp(-\beta\ u*^{0.5}\theta*^{0.25})}\right)$
kB_m^{-1}	kB^{-1} for mixed bare-soil and canopy	$\frac{k\frac{u*}{u(h)}\frac{z_{0m}}{h}}{C_t^*}$	Same as SEBS, with different $\frac{u*}{u(h)}$ and $\frac{z_{0m}}{h}$
$\frac{u*}{u(h)}$	representation of surface drag coefficient	$C_1-C_2\exp(-C_3\,C_d\,LAI)$	$C_1-C_2\exp(-C_3\,\zeta(h))$
n_{ec}	wind speed extinction coefficient within-canopy	$\frac{C_d\ \text{LAI}}{2(C_1-C_2\ \exp(-C_3\ C_d\ \text{LAI}))})^2$, C_1 =0.320, C_2 =0.264, and C_3 =15.1	$\frac{\zeta(h)}{2(C_1-C_2\ \exp(-C_3\ \zeta(h)))^2}$, C_1= 0.320, C_2 =0.264, and C_3 =15.1
$\zeta(z)$	cumulative leaf drag area per unit planform area	Not used	$\int_0^z[a(z')\ C_d^v(z')\ P_m^v(z')]dz'$

Table 2 *(continued)*

Symbol	Description	SEBS	This study
$a(\xi)$	foliage leaf area density function	Not used	$\frac{LAI}{h}\frac{\beta(\xi)}{\int_0^1\beta(\xi)d\xi}$
$C_d^v(\xi)$	foliage drag coefficient in the canopy	Not used	$C_d e^{-A2(1-\xi)}$
$P_m^v(\xi)$	foliage shelter factor for momentum	Not used	$1/(1+0.4\,h\,a(\xi))$
$\beta(\xi)$	shape of foliage leaf area density function	Not used	$\begin{cases}\exp(-(\xi-\xi_m)^2/\sigma_u^2) & \xi_m\le\xi\le1\\ \exp(-(\xi_m-\xi)^2/\sigma_l^2) & 0\le\xi\le\xi_m\end{cases}$
ξ_m	height of maximum foliage area density	Not used	Different land covers have different values
σ_u	standard deviation of foliage density profile in the upper layer above ξ_m	Not used	Different canopy has different values
σ_l	standard deviation of foliage density profile in lower layer below ξ_m	Not used	Different canopy has different values.
A_2	Vertical canopy momentum drag coefficient	Not used	A2 = −1 to emulate the case when drag coefficient decreases with increasing wind speed, while A2 = 1 is used for the case when the drag coefficient increases with increasing wind speed. A2 = −5 was used in this study.

methods for $a(z')$, $C_d^v(z')$, and $P_m^v(z')$ were used in this study, while $C_d^v(z')$ and $P_m^v(z')$ were set as a constant values of 0.2 and 1 in Su et al. (2001).

$$a(\xi)=\frac{\mathrm{LAI}}{h}\,\frac{\beta(\xi)}{\int_0^1\beta(\xi)d\xi}, \tag{17}$$

$$C_d^v(\xi)=C_d e^{-A2(1-\xi)}, \tag{18}$$

with $\xi=z/h$; A2 = −1 to emulate the case when drag coefficient decreases with increasing wind speed, while A2 = 1 is used for the case when the drag coefficient increases with increasing wind speed (Massman & Weil, 1999). A *asymmetric Gaussian* method for $\beta(\xi)$ from Massman et al. (2017) has been used in this study, which can be more easily defined for any kind of canopies than the beta function used in Su et al. (2001):

$$\beta(\xi)=\begin{cases}\exp(-(\xi-\xi_m)^2/\sigma_u^2) & \xi_m\le\xi\le1\\ \exp(-(\xi_m-\xi)^2/\sigma_l^2) & 0\le\xi\le\xi_m\end{cases}, \tag{19}$$

with ξ_m as the height of maximum foliage area density and σ_u and σ_l are the standard deviation of foliage density profile in the upper layer above ξ_m and lower layer below ξ_m. An asymmetric Gaussian is used in equation (19) as it provides smoother canopy wind and stress profiles, as well as a smoother $\beta(\xi)$, without compromising the model's performance.

Table 3
List of ξ_m (Height of Maximum Foliage Area Density), and σ_u and σ_l (the Standard Deviation of Foliage Density Profile in the Upper Layer and Lower Layer), Leaf Drag Coefficient, and Foliage Shelter Parameters (A2 and A_s)

	ENF	DBF	SRB	SAV	GRS	CRP	BSN
ξ_m	0.6	0.55	0.95	0.40	0.99	0.72	0.9
σ_u	0.18	0.40	0.35	0.15	0.55	0.01	0.14
σ_l	0.06	0.30	0.001	0.05	0.03	0.001	0.001
A_s	0.5	0.5	0.5	0.5	0.5	0.5	0.5
A2	−5	−5	−5	−5	−5	−5	−5

Note. BSN, barren; CRP, croplands; DBF, deciduous broadleaf forest; ENF, evergreen needleleaf forest; GRS, grasslands; SAV, savannas; SRB, shrub-land.

Sheltering occurs when neighboring canopy elements interfere with one another. One canopy element may block or reduce the exposure of another neighboring element to the turbulent wind. Consequently, $P_m^v(z)$ might be expected to decrease with increasing of foliage density. Hereby $P_m^v(z)$ is calculated by the method of Massman and Weil (1999) as:

$$P_m^v(\xi)=1/(1+A_s\,\mathrm{h}\,a(\xi)) \tag{20}$$

The values of A_s for different canopies are listed in Table 3. A constant value for A2 was used as discussed above. The chosen values for A_s and A2 can provide satisfactory H estimates, but they may be optimized based on stability in future work.

The within-canopy wind momentum transfer model represented by equations (15)–(20) is further used to estimate d and z_{0m}. Su02 and Chen13 used the following method to calculate d:

$$\frac{d}{h} = 1 - \int_0^1 e^{-2\, n_{ec}(1-\zeta(z)/\zeta(h))} d\xi, \tag{21}$$

A more physically realistic method for $\frac{d}{h}$ (Jackson, 1981; Massman et al., 2017; Seginer, 1974) was used for canopies of arbitrary plant surface distribution and leaf area and can reproduce observed canopy wind speed profiles across a wide variety of canopies. As within-canopy Reynolds stress, $u_*^2(z)$, provides a reasonable description of the observed vertical profiles of Reynolds stress, it is used by this study to calculate z_{0m} and d.

$$\frac{z_{0m}}{h} = \left(1 - \frac{d}{h}\right) e^{-k\, u(h)/u_*}, \tag{22}$$

$$\frac{d}{h} = \left(1 - \frac{u_*^2(0)}{u_*^2(1)}\right) \frac{\int_0^1 \left[u_*^2(\xi)/u_*^2(1)\right] \xi d\xi}{\int_0^1 \left[u_*^2(\xi)/u_*^2(1)\right] d\xi}, \tag{23}$$

Readers are referred to Jackson (1981), Massman et al. (2017), and Seginer (1974) for the calculation of $u_*^2(0)$, $u_*^2(1)$, and $u_*^2(\xi)$.

Linking to equation (12b), (16), and (22), it can be deduced that the estimates of z_{0m}/h and d/h are only based on the variation of normalized $\zeta(z)$, which is determined by the vertical variations of foliage density, foliage drag coefficient, and foliage shelter factor inside the canopy.

3.3.2. Revision of Foliage Heat Transfer Coefficient

The foliage heat transfer coefficient is closely related to canopy-air heat transfer. In previous versions of Su02 and Chen13, C_t in equation (12a)) is given a constant value of 0.01. However, the foliage heat transfer coefficient should vary with the turbulent intensity within the canopy. Hereby a solution to include the vertical variation of C_t in the canopy is provided. Brutsaert (1979) suggested

$$C_{tf} = C_L\, P_r^{-m}\, \mathrm{Re}_*^{-n}, \tag{24}$$

C_L, m, and n are parameters that may depend on the shape, density, and orientation of the leaves and on the intensity of the turbulence. Re_* is a local canopy Reynolds number, which can be calculated with either friction velocity or wind speed. Here local canopy Reynolds number is calculated with wind speed profile in the canopy, as $\mathrm{Re}_*(z) = l * u(z)/\vartheta$. l is the characteristic leaf length scale [0.01 m]; $u(z)$ is the wind speed in the canopy. If wind speed is used as velocity scale for Re_*,the parameter C_L should be adjusted to be $[u_*/u(h)]^{0.5}$ (Brutsaert, 1979). The wind speed profile in the canopy can be derived from the above mentioned column canopy-air turbulent transfer model, as shown in the equation (15). $u(z)$ is used to calculate local canopy Reynolds number or leaf Reynolds number for each vertical canopy layers ($\mathrm{Re}_*(z)$); by doing so a vertical profile of foliage heat transfer efficiency in the canopy ($C_t^v(z)$) can be derived by

$$C_t^v(z) = [u_*/u(h)]^{0.5} * \mathrm{Pr}^{-0.67} * \mathrm{Re}_*(z)^{-0.5} \tag{25}$$

The relation between turbulent Prandtl number (Pr) and atmospheric stability in Li et al. (2015) also has a potential to be applied for $C_t^v(z)$ calculation. An average vertical foliage heat transfer value $C_t = \overline{C_t^v(z)}$ is then used to calculate kB_c^{-1} and further kB^{-1}. The results of using the new C_t scheme (labeled by *this paper*) and a constant C_t value of 0.01 (labeled by *Su02* and *Chen13*) are shown in Figure 2. Su02 and Chen13 refer to results by a different kB^{-1}model from this paper with a C_t value of 0.01. The comparison between the three schemes shows that the new model developed by this study has the best performance for sensible heat flux simulation. The enhanced performance of the new model explained that the addition of vertical foliage density, vertical foliage drag coefficient, and vertical foliage heat transfer efficiency in the canopy is necessary for correct simulation of turbulent heat flux over high canopy.

Figures 3 and 4 also describe the impact of the model rebuilt by this study. kB_c^{-1} significantly decreased in the new model. kB^{-1} at the two forest sites from the new model is not higher than 3. The lower kB^{-1} in the new

model could solve H underestimates at forest sites. Meanwhile, the new model retains a similar performance at nonforest sites. The RMSE at Speulderbos and US-UMB forest sites have been reduced from 93.4 and 141.1 to 70.6 and 74.9 W/m^2, respectively. Our tests show that the revision to foliage heat transfer coefficient is most important to the H improvement.

4. Discussions

In practice, kB^{-1} is derived from the bulk transfer formulation using measurements of other quantities. Any uncertainties associated with these measurements will cause uncertainties in the evaluation of kB^{-1} and the estimated sensible heat flux. The flux and meteorological variables may have different up-wind source area than that of the foliage temperature due to different measurement heights and the involved processes. A more critical selection of high-quality turbulent flux with statistically stationary and horizontal homogeneity analysis (Foken & Wichura, 1996) may help to get a better model performance. The surface temperature was determined using radiometers with a limited field of view. An assumption was made to regard this temperature as representative of the fetch area of the EC system and can represent the mean status of whole canopy foliage layers. The discrepancy shown by the scatter plot in Figure 2 is believed to be related to differences in footprint of the sensors and caused by effects of the inhomogeneous terrain. Troufleau et al. (1997) noted that the notion of *surface* over forest canopy is quite problematic compared with bare soil. In fact, the only observation technique available to determine leaf surface temperature for us to use Fluxnet data is that from a radiometer. Radiometric surface temperatures are derived from measurements of the radiance emitted by everything within the field of view of the sensor. For a flat soil surface, the radiance is emitted from the plane of the surface. Vegetated surfaces present greater complications, especially when the vegetation is bluff rough and has a permeable rough surface (Bosveld, 1999). In the case of sparse canopy there are indications that this technique is inadequate, because a radiometer could see too much understory or bare surface, and does not yield the temperature of the vegetation surface that drives the sensible heat flux. As a result, the surface temperature observed with a radiometer is smaller than the air temperature above the trees. On the other hand, the observed sensible heat flux could be positive—that is, a heat flux goes from the surface into the air. This will also cause difficulties in the simulation of sensible heat over forest and explain why forest sites have relative high RMSE in Figure 5. Furthermore, in order to upscale the canopy turbulent transfer model to global area, a 5 × 5 km LAI, NDVI pixel value is used to represent LAI and NDVI variation for the station location. This also introduces a certain error in kB^{-1} and H estimates.

Calculation of H using the MOST approach over tall canopy areas is well known to underestimate sensible heat flux (Mölder et al., 1999). Due to a roughness sublayer, which exists just above a forest stand, eddy diffusivities in the roughness sublayer are enhanced and gradients of meteorological variables are reduced. The traditional surface layer relationships are satisfied only at heights sufficiently above the roughness elements. We have examined a roughness scheme from Physick and Garratt (1995) by using 28 flux tower measurements. The meteorological measurements at 11 forest flux sites are within the roughness sublayer above the canopy. Previous studies have shown that fluxes calculated from profiles by a method, which takes into account the roughness sublayer corrections, are generally in good agreement with those measured by the EC method within the roughness sublayer. Several suggestions of corrections to the standard flux-profile expression have been proposed in order to increase the magnitude of turbulent heat flux (Arnqvist & Bergström, 2015; Graefe, 2004; Harman & Finnigan, 2007). The column canopy-air turbulent diffusion method developed in this study takes into account the impact of forest canopy on the vertical profile by calculating the vertical variation of u_* and u in the canopy. The vertical variations of u_* and u have been included in the calculation of d_0, z_{0m}, kB_c^{-1}, kB_m^{-1}, kB^{-1}, and z_{0h}. Thus, the roughness sublayer impact is represented in the model but not by a canopy-mixing-layer length scale. The vertical variation of u_* has also been used in the calculation of the heat transfer coefficient in this study. This is why our model has similar performance as that of a subroughness length stability calibration method in other studies (Cellier & Brunet, 1992; Mölder et al., 1999). Furthermore, we also tested the subroughness length stability calibration in the model. Meanwhile, adding or not-adding the calibration is nearly the same as shown by Figure 5. The reason could be due to using the same subroughness correction function as Physick and Garratt (1995), which may need to be adjusted at each site. A fixed ratio of Z^* to canopy height was used in this study, and we did not optimize

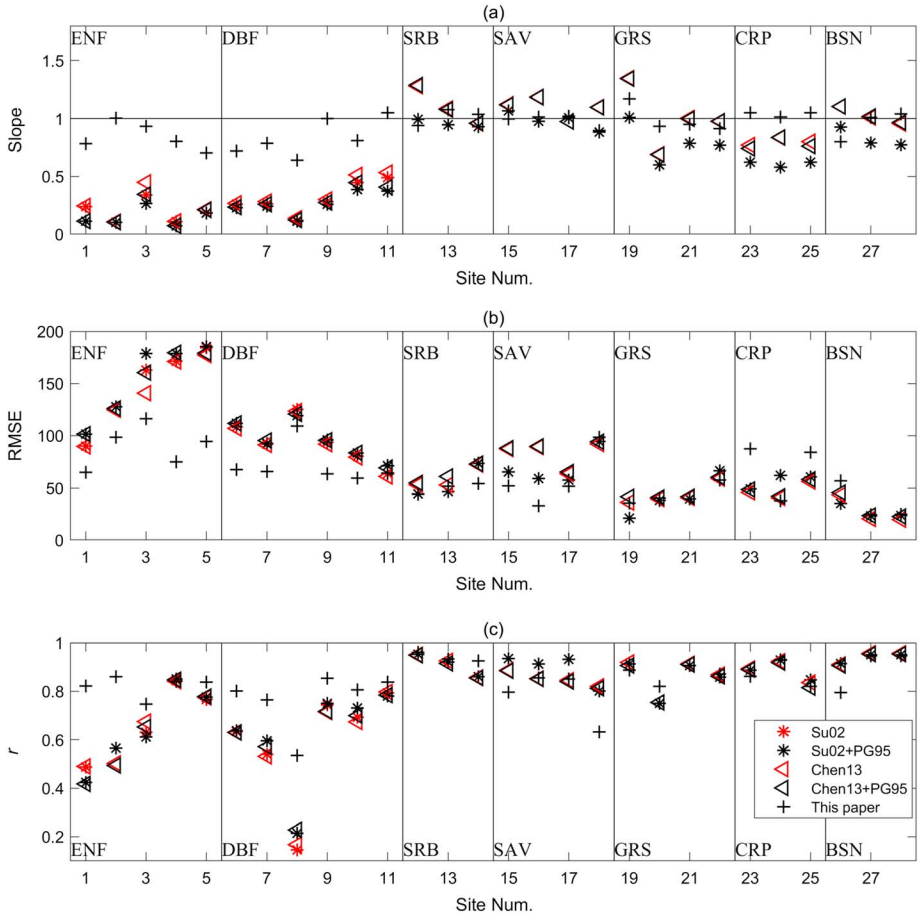

Figure 5. The (a) linear fitting slope, (b) root-mean-square error (RMSE), and (c) r derived from H observation and simulation with four schemes. Su02 + PG95 means roughness scheme from SEBS (Su, 2002), and the subroughness correction function from Physick and Garratt (1995) were used. Chen13 + PG95 means roughness scheme from Chen et al. (2013), and the subroughness correction function from Physick and Garratt (1995) were used.

the value of Z^*, ϕ_s, ϕ_u, Φ_s, and Φ_u for each site. Nevertheless, the new model now provides a generally better result than the previous two versions, shown by a lower RMSE, higher r, and slope value closer to 1 (Figure 5). Site numbers 23 and 25 demonstrate the new model with a slightly higher RMSE, while its slope values show better results than other versions. Site numbers 15 and 18 have a lower r value, while their RMSE and slope demonstrate a better performance. It is more interesting for us to look at slope values, since previous model version has achieved a clear low bias. The slope values at the 28 sites indicate the progress made in this paper. In addition, both RMSEs for 22 sites and r for 25 sites show that the new model is better than previous versions. Thus, the bias at a few sites need not influence the conclusion of the generally better performance of the new model.

For global flux calculation, the same values for ξ_m, σ_u, σ_l, and A_s listed in Table 3 can be used for the same land covers. In future, the leaf area density profile at global scale will be produced by satellite lidar sensors. Tang et al. (2016) have demonstrated the capability of mapping leaf area density over the United States, using satellite lidar technology. Once global maps of leaf area density information become available, the need for the asymmetric Gaussian function may be reduced for estimation of the canopy-air flux.

5. Conclusions

Flux parameterization in the atmospheric surface layer is one of the most used methods in numerical weather prediction models because of its ease of use and effectiveness in the quantification of turbulent exchange processes between the Earth's surface and the lower atmosphere. However, the classical flux-

gradient relationships derived from the surface layer similarity theory have been known for a long time to be not valid in the so-called *roughness sublayer*, the layer just above plant canopies (Cellier & Brunet, 1992). Noticeable discrepancies have been reported by many authors between flux values derived from the surface layer similarity theory and those measured by EC technique. This was also found by us over forests when using a kB^{-1} scheme in MOST. The bulk transfer equation based on the MOST provides a relatively simple way to parameterize land-atmosphere heat transfer. However, this approach requires an estimate of roughness length and kB^{-1}. Different approximations of roughness length can cause considerable changes in the estimation of turbulent fluxes at the surface. Usually, the surface roughness length is given a fixed value in numerical models but is widely known to be varying in space and time. Many numerical weather prediction models have substantial biases in the radiative surface temperature (Chen et al., 2017), due to biases in the choice of kB^{-1}. A previous kB^{-1} model has been enhanced in this study to make it suitable for high and low canopies, allowing the use of the aerodynamic method over different canopies. This kB^{-1} parameterization model was driven by a time series of meteorological observation data at point scales, and its performance has been evaluated by comparisons between its simulated sensible heat fluxes and observed ones at 28 flux stations. The measurements were performed over seven typical land-cover types that cover the major land areas. The results show that the Su02 and Chen13 formulation of kB^{-1} (used in the SEBS model) tends to produce underestimates for H over forest canopy covers. Using sensitivity analyses, the most critical parameters (foliage drag coefficient and heat transfer coefficient of the leaf) for kB^{-1} estimation have been identified. The model structure is revised in this study from one foliage layer concept in SEBS to a vertical foliage layers model. The wind speed profile extinction coefficient within the canopy proposed by Massman (1997) has been used to rebuild the model as a column canopy-air turbulent transfer model. The new model was found to be more robust over bare soil, short canopy, and tall canopies.

As Physick and Garratt (1995) pointed out that there are two methods that solve the presence of high roughness over forest covers in the land-air turbulent flux calculation. The first method parameterizes the mean flow and turbulent exchange fluxes within the forest. The second approach is to treat the forest as a very rough surface, which takes into account the effect of forest high roughness by using subroughness length stability calibration. This paper used both methods to solve the underestimation problem in sensible heat flux simulation and reported that the first method is more accurate.

This paper has shown that a more physical expression of important parameters, such as foliage drag coefficient, heat transfer coefficient of the leaf, based on process studies, may significantly improve the model simulation. A quick solution to solve the underestimation of H can be the optimization of the values for parameters C_t, C_d, and C_1 in respect of canopy classification. However, a universal representation of the physical process and the parameters would be preferable, because the universal physical process representation is closer to reality. Another possible solution could be to use a macroscopic relation between the turbulent Prandtl number and atmospheric stability (Li et al., 2015), which might give an accurate H estimation. This study also found that the model overestimates H during stable conditions at nighttime; this might need further investigation.

Equation (11) is a simple description of the combined effects of the canopy and soil boundary layer on kB^{-1}, which uses the canopy fraction as a weighting factor for canopy and the soil boundary layer resistance in the full LNF model. The final flux calculation method uses the one source method, and this study has demonstrated that revisions to canopy effects on kB^{-1} could improve the one source simulation of canopy-air turbulent heat transfer.

The new updated scheme of turbulent heat flux parameterization method will be useful for land-surface interaction simulations in weather and climate models. This work advances the model proposed by Su02 and Chen13 to be applicable for typical land covers of the globe and helps us to analyze the possibility and suitability to generate surface heat flux maps over global land areas by remote sensing techniques, which has been the subject of the study by the Energy and Water Cycle Study (NEWS) of the National Aeronautics and Space Administration (NASA), the Integrated Land Ecosystem-Atmosphere Process study (iLEAPS), the EU Water and Global Change (WATCH), the Water Cycle Multimission Observation Strategy (WACMOS) by the European Space Agency (ESA), and the LandFlux-EVAL initiative of the Global Energy and Water Cycle Experiment (GEWEX).

Acknowledgments
Xuelong Chen was supported by CAS Pioneer Hundred Talents Program. We acknowledge the following AmeriFlux sites: sites Us-NC2, US-GLE, US-MRf, US-NR1, US-UMB, US-ChR, US-MOz, US-MMS, US-WBW, US-WCr, US-Aud, US-Me6, US-Fmf, Us-Br1, US-Ctn, and US-Wkg, and the following TERN OzFlux sites: Gingin, Calperum, Ti Tree East, Riggs Creek, Daly Pasture, and Arcturus, for providing us with their data sets. The flux tower data and model code could be downloaded from https://github.com/TSEBS/A-column-canopy-air-turbulent-heat-diffusion-model.

References

Albini, F. A. (1981). A phenomenological model for wind speed and shear stress profiles in vegetation cover layers. *Journal of Applied Meteorology*, *20*(11), 1325–1335. https://doi.org/10.1175/1520-0450(1981)020<1325:APMFWS>2.0.CO;2

Arnqvist, J., & Bergström, H. (2015). Flux-profile relation with roughness sublayer correction. *Quarterly Journal of the Royal Meteorological Society*, *141*(689), 1191–1197. https://doi.org/10.1002/qj.2426

Banerjee, T., De Roo, F., & Mauder, M. (2017). Explaining the convector effect in canopy turbulence by means of large-eddy simulation. *Hydrology and Earth System Sciences*, *21*(6), 2987–3000. https://doi.org/10.5194/hess-21-2987-2017

Beljaars, A. C. M., & Holtslag, A. A. M. (1991). Flux parameterization over land surfaces for atmospheric models. *Journal of Applied Meteorology*, *30*(3), 327–341. https://doi.org/10.1175/1520-0450(1991)030<0327:FPOLSF>2.0.CO;2

Bosveld, F.C., 1999. Exchange processes between a coniferous forest and the atmosphere, Wageningen University, 181 pp.

Brutsaert, W. (1979). Heat and mass transfer to and from surfaces with dense vegetation or similar permeable roughness. *Boundary-Layer Meteorology*, *16*(3), 365–388. https://doi.org/10.1007/BF03335377

Brutsaert, W. (Ed) (1982). *Evaporation into the atmosphere* (p. 299). Dordrecht: D. Reidel. https://doi.org/10.1007/978-94-017-1497-6

Brutsaert, W. (2010). *Evaporation into the atmosphere: Theory, history and applications*. Netherlands: Springer.

Brutsaert, W., & Sugita, M. (1996). Sensible heat transfer parameterization for surfaces with anisothermal dense vegetation. *Journal of the Atmospheric Sciences*, *53*(2), 209–216. https://doi.org/10.1175/1520-0469(1996)053<0209:SHTPFS>2.0.CO;2

Burba, G. G., McDermitt, D. K., Anderson, D. J., Furtaw, M. D., & Eckles, R. D. (2010). Novel design of an enclosed CO_2/H_2O gas analyser for eddy covariance flux measurements. *Tellus B*, *62*(5), 743–748. https://doi.org/10.1111/j.1600-0889.2010.00468.x

Cellier, P., & Brunet, Y. (1992). Flux-gradient relationships above tall plant canopies. *Agricultural and Forest Meteorology*, *58*(1–2), 93–117. https://doi.org/10.1016/0168-1923(92)90113-I

Chen, X., Su, Z., Ma, Y., Cleverly, J., & Liddell, M. (2017). An accurate estimate of monthly mean land surface temperatures from MODIS clear-sky retrievals. *Journal of Hydrometeorology*, *18*(10), 2827–2847. https://doi.org/10.1175/JHM-D-17-0009.1

Chen, X., Su, Z., Ma, Y., Liu, S., Yu, Q., & Xu, Z. (2014). Development of a 10-year (2001–2010) 0.1° data set of land-surface energy balance for mainland China. *Atmospheric Chemistry and Physics*, *14*(23), 13,097–13,117. https://doi.org/10.5194/acp-14-13097-2014

Chen, X., Su, Z., Ma, Y., Yang, K., Wen, J., & Zhang, Y. (2013). An improvement of roughness height parameterization of the Surface Energy Balance System (SEBS) over the Tibetan Plateau. *Journal of Applied Meteorology and Climatology*, *52*(3), 607–622. https://doi.org/10.1175/JAMC-D-12-056.1

Choudhury, B. J., & Monteith, J. L. (1988). A four-layer model for the heat budget of homogeneous land surfaces. *Quarterly Journal of the Royal Meteorological Society*, *114*(480), 373–398. https://doi.org/10.1002/qj.49711448006

De Ridder, K. (2010). Bulk transfer relations for the roughness sublayer. *Boundary-Layer Meteorology*, *134*(2), 257–267. https://doi.org/10.1007/s10546-009-9450-y

Ershadi, A., McCabe, M. F., Evans, J. P., Chaney, N. W., & Wood, E. F. (2014). Multi-site evaluation of terrestrial evaporation models using FLUXNET data. *Agricultural and Forest Meteorology*, *187*, 46–61. https://doi.org/10.1016/j.agrformet.2013.11.008

Feng, J., Liu, H., Wang, L., Du, Q., & Shi, L. (2012). Seasonal and inter-annual variation of surface roughness length and bulk transfer coefficients in a semiarid area. *Science China Earth Sciences*, *55*(2), 254–261. https://doi.org/10.1007/s11430-011-4258-2

Flerchinger, G. N., Reba, M. L., & Marks, D. (2012). Measurement of surface energy fluxes from two rangeland sites and comparison with a multilayer canopy model. *Journal of Hydrometeorology*, *13*(3), 1038–1051. https://doi.org/10.1175/JHM-D-11-093.1

Foken, T., & Wichura, B. (1996). Tools for quality assessment of surface-based flux measurements. *Agricultural and Forest Meteorology*, *78*(1–2), 83–105. https://doi.org/10.1016/0168-1923(95)02248-1

Garratt, J. R. (1978). Flux profile relations above tall vegetation. *Quarterly Journal of the Royal Meteorological Society*, *104*(439), 199–211. https://doi.org/10.1002/qj.49710443915

Garratt, J. R. (1980). Surface influence upon vertical profiles in the atmospheric near-surface layer. *Quarterly Journal of the Royal Meteorological Society*, *106*(450), 803–819. https://doi.org/10.1002/qj.49710645011

Garratt, J. R., & Hicks, B. B. (1973). Momentum, heat and water vapour transfer to and from natural and artificial surfaces. *Quarterly Journal of the Royal Meteorological Society*, *99*(422), 680–687. https://doi.org/10.1002/qj.49709942209

Graefe, J. (2004). Roughness layer corrections with emphasis on SVAT model applications. *Agricultural and Forest Meteorology*, *124*(3–4), 237–251. https://doi.org/10.1016/j.agrformet.2004.01.003

Harman, I., & Finnigan, J. (2008). Scalar concentration profiles in the canopy and roughness sublayer. *Boundary-Layer Meteorology*, *129*(3), 323–351. https://doi.org/10.1007/s10546-008-9328-4

Harman, I. N., & Finnigan, J. J. (2007). A simple unified theory for flow in the canopy and roughness sublayer. *Boundary-Layer Meteorology*, *123*(2), 339–363. https://doi.org/10.1007/s10546-006-9145-6

Hong, J., Kim, J., & Byun, Y. H. (2012). Uncertainty in carbon exchange modelling in a forest canopy due to kB−1 parametrizations. *Quarterly Journal of the Royal Meteorological Society*, *138*(664), 699–706. https://doi.org/10.1002/qj.944

Jackson, P. S. (1981). On the displacement height in the logarithmic velocity profile. *Journal of Fluid Mechanics*, *111*(1), 15–25. https://doi.org/10.1017/S0022112081002279

Jensen, N. O., & Hummelshøj, P. (1995). Derivation of canopy resistance for water vapour fluxes over a spruce forest, using a new technique for the viscous sublayer resistance. *Agricultural and Forest Meteorology*, *73*(3–4), 339–352. https://doi.org/10.1016/0168-1923(94)05083-I

Li, D., Katul, G. G., & Zilitinkevich, S. S. (2015). Revisiting the turbulent Prandtl number in an idealized atmospheric surface layer. *Journal of the Atmospheric Sciences*, *72*(6), 2394–2410. https://doi.org/10.1175/JAS-D-14-0335.1

Ma, Y., Kang, S., Zhu, L., Xu, B., Tian, L., & Yao, T. (2008). Tibetan observation and research platform—Atmosphere–land interaction over a heterogeneous landscape. *Bulletin of the American Meteorological Society*, *89*, 1487–1492.

Massman, W. J. (1997). An analytical one-dimensional model of momentum transfer by vegetation of arbitrary structure. *Boundary-Layer Meteorology*, *83*(3), 407–421. https://doi.org/10.1023/A:1000234813011

Massman, W. J. (1999). A model study of kBH−1 for vegetated surfaces using 'localized near-field' Lagrangian theory. *Journal of Hydrology*, *223*(1–2), 27–43. https://doi.org/10.1016/S0022-1694(99)00104-3

Massman, W. J., Forthofer, J. M., & Finney, M. A. (2017). An improved canopy wind model for predicting wind adjustment factors and wildland fire behavior. *Canadian Journal of Forest Research*, *47*(5), 594–603. https://doi.org/10.1139/cjfr-2016-0354

Massman, W. J., & Weil, J. C. (1999). An analytical one-dimensional second-order closure model of turbulence statistics and the Lagrangian time scale within and above plant canopies of arbitrary structure. *Boundary-Layer Meteorology*, *91*(1), 81–107. https://doi.org/10.1023/A:1001810204560

McNaughton, K. G., & van den Hurk, B. J. J. M. (1995). A 'Lagrangian' revision of the resistors in the two-layer model for calculating the energy budget of a plant canopy. *Boundary-Layer Meteorology*, *74*(3), 261–288. https://doi.org/10.1007/BF00712121

Mölder, M., Grelle, A., Lindroth, A., & Halldin, S. (1999). Flux-profile relationships over a boreal forest—Roughness sublayer corrections. *Agricultural and Forest Meteorology*, *98–99*, 645–658.

Oku, Y., Ishikawa, H., & Su, Z. (2007). Estimation of land surface heat fluxes over the Tibetan plateau using GMS data. *Journal of Applied Meteorology and Climatology*, *46*(2), 183–195. https://doi.org/10.1175/JAM2456.1

Owen, P. R., & Thomson, W. R. (1963). Heat transfer across rough surfaces. *Journal of Fluid Mechanics*, *15*(03), 321–334. https://doi.org/10.1017/S0022112063000288

Physick, W. L., & Garratt, J. R. (1995). Incorporation of a high-roughness lower boundary into a mesoscale model for studies of dry deposition over complex terrain. *Boundary-Layer Meteorology*, *74*(1-2), 55–71. https://doi.org/10.1007/BF00715710

Qualls, R. J., & Brutsaert, W. (1996). Effect of vegetation density on the parameterization of scalar roughness to estimate spatially distributed sensible heat fluxes. *Water Resources Research*, *32*, 645–652. https://doi.org/10.1029/95WR03097

Raupach, M. R. (1989). Applying Lagrangian fluid mechanics to infer scalar source distributions from concentration profiles in plant canopies. *Agricultural and Forest Meteorology*, *47*(2-4), 85–108. https://doi.org/10.1016/0168-1923(89)90089-0

Raupach, M. R. (1994). Simplified expressions for vegetation roughness length and zero-plane displacement as functions of canopy height and area index. *Boundary-Layer Meteorology*, *71*(1–2), 211–216. https://doi.org/10.1007/BF00709229

Rotenberg, E., & Yakir, D. (2010). Contribution of semi-arid forests to the climate system. *Science*, *327*(5964), 451–454. https://doi.org/10.1126/science.1179998

Saha, K. (2008). *The Earth's atmosphere: Its physics and dynamics*. Berlin Heidelberg: Springer.

Schaudt, K. J., & Dickinson, R. E. (2000). An approach to deriving roughness length and zero-plane displacement height from satellite data, prototyped with BOREAS data. *Agricultural and Forest Meteorology*, *104*(2), 143–155. https://doi.org/10.1016/S0168-1923(00)00153-2

Seginer, I. (1974). Aerodynamic roughness of vegetated surfaces. *Boundary-Layer Meteorology*, *5*(4), 383–393. https://doi.org/10.1007/BF00123487

Su, H., McCabe, M. F., Wood, E. F., Su, Z., & Prueger, J. H. (2005). Modeling evapotranspiration during SMACEX: Comparing two approaches for local- and regional-scale prediction. *Journal of Hydrometeorology*, *6*(6), 910–922. https://doi.org/10.1175/JHM466.1

Su, Z. (2002). The Surface Energy Balance System (SEBS) for estimation of turbulent heat fluxes. *Hydrology and Earth System Sciences*, *6*(1), 85–100. https://doi.org/10.5194/hess-6-85-2002

Su, Z., Schmugge, T., Kustas, W. P., & Massman, W. J. (2001). An evaluation of two models for estimation of the roughness height for heat transfer between the land surface and the atmosphere. *Journal of Applied Meteorology*, *40*(11), 1933–1951. https://doi.org/10.1175/1520-0450(2001)040<1933:AEOTMF>2.0.CO;2

Su, Z., Timmermans, W. J., van der Tol, C., Dost, R., Bianchi, R., Gómez, J. A., et al. (2009). EAGLE 2006 – Multi-purpose, multi-angle and multi-sensor in-situ and airborne campaigns over grassland and forest. *Hydrology and Earth System Sciences*, *13*(6), 833–845. https://doi.org/10.5194/hess-13-833-2009

Sun, J. (1999). Diurnal variations of thermal roughness height over a grassland. *Boundary-Layer Meteorology*, *92*(3), 407–427. https://doi.org/10.1023/A:1002071421362

Tang, H., Ganguly, S., Zhang, G., Hofton, M. A., Nelson, R. F., & Dubayah, R. (2016). Characterizing leaf area index (LAI) and vertical foliage profile (VFP) over the United States. *Biogeosciences*, *13*, 239–252.

Thom, A. S. (1972). Momentum, mass and heat exchange of vegetation. *Quarterly Journal of the Royal Meteorological Society*, *98*(415), 124–134. https://doi.org/10.1002/qj.49709841510

Troufleau, D., Lhomme, J. P., Monteny, B., & Vidal, A. (1997). Sensible heat flux and radiometric surface temperature over sparse Sahelian vegetation. I. An experimental analysis of the kB−1 parameter. *Journal of Hydrology*, *188–189*, 815–838.

Verhoef, A., De Bruin, H. A. R., & Van Den Hurk, B. J. J. M. (1997). Some practical notes on the parameter kB−1 for sparse vegetation. *Journal of Applied Meteorology*, *36*(5), 560–572. https://doi.org/10.1175/1520-0450(1997)036<0560:SPNOTP>2.0.CO;2

Verhoef, A., McNaughton, K. G., & Jacobs, A. F. G. (1997). A parameterization of momentum roughness length and displacement height for a wide range of canopy densities. *Hydrology and Earth System Sciences*, *1*(1), 81–91. https://doi.org/10.5194/hess-1-81-1997

Vinukollu, R. K., Meynadier, R., Sheffield, J., & Wood, E. F. (2011). Multi-model, multi-sensor estimates of global evapotranspiration: Climatology, uncertainties and trends. *Hydrological Processes*, *25*(26), 3993–4010. https://doi.org/10.1002/hyp.8393

Wang, S., & Ma, Y. (2011). Characteristics of land–atmosphere interaction parameters over the Tibetan Plateau. *Journal of Hydrometeorology*, *12*(4), 702–708. https://doi.org/10.1175/2010JHM1275.1

Webb, E. K., Pearman, G. I., & Leuning, R. (1980). Correction of flux measurements for density effects due to heat and water vapour transfer. *Quarterly Journal of the Royal Meteorological Society*, *106*(447), 85–100.

Yang, K., Koike, T., Fujii, H., Tamagawa, K., & Hirose, N. (2002). Improvement of surface flux parametrizations with a turbulence-related length. *Quarterly Journal of the Royal Meteorological Society*, *128*(584), 2073–2087. https://doi.org/10.1256/003590002320603548

Yang, K., Koike, T., & Yang, D. (2003). Surface flux parameterization in the Tibetan plateau. *Boundary-Layer Meteorology*, *106*(2), 245–262. https://doi.org/10.1023/A:1021152407334